On the Hyperspectral Modeling of Light Interaction with Human Skin

T. Francis Chen, Gladimir V. G. Baranoski, Bradley Kimmel, Erik Miranda

CS-2013-14

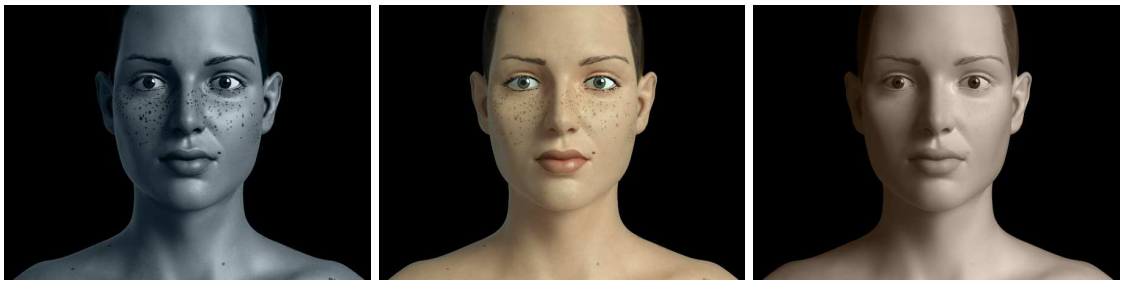

Figure 1: Images showing distinct skin appearance features in the ultraviolet (left), visible (middle) and infrared (right) spectral domains. These images were rendered using BSSRDF representations of spatial light distributions provided by HyLIoS. The ultraviolet and infrared responses (at 365 nm and 1100 nm, respectively) are depicted using pseudo color.

Abstract

The exploration of the hyperspectral domain offers a host of new research and application possibilities in terms of material appearance modeling. In this paper, we address these prospects with respect to human skin, one of the most ubiquitous materials portrayed in synthetic imaging. We present a novel hyperspectral skin appearance model that takes into account the optical and structural characteristics of this complex organ as well as the particle nature of its main light-attenuation agents to enable the predictive rendering of its appearance attributes in the ultraviolet, visible and infrared regions of the light spectrum. Accordingly, it has a broad scope of applications involving hyperspectral skin imaging for entertainment, aesthetic, educational and biomedical purposes. The predictions of the proposed model are quantitatively and qualitatively evaluated through comparisons with measured data. In addition, its effectiveness is further illustrated through the generation of images depicting distinct trends in the variation of skin appearance attributes detected under visible and non-visible light.

1 Introduction

In the last decades, significant advances have been achieved in the modeling of material appearance, with sophisticated appearance models being developed for a wide range of materials [DRS07]. Due

to its inherent optical complexity, human skin represents an ongoing challenge in this area. To date, the bulk of the work on light and skin interactions within the computer graphics field has been aimed at skin imaging in the visible domain. As a result, existing skin appearance models have been successfully employed in image synthesis applications [JB03, TOS*03, DWd*08, JSB*10] as well as in biomedical investigations [BCK*12, CSB13] centered at the visible appearance attributes of human skin. However, there are still relevant avenues of research associated with skin appearance that remain unexplored, notably with respect to the hyperspectral modeling of light and skin interactions, spanning from the ultraviolet (UV) to the infrared (IR) domains.

The investigation of phenomena affecting material appearance attributes within a broader hyperspectral domain can lead to important interdisciplinary contributions in physical and life sciences as demonstrated by recent computer graphics works in this area [KR11, KHK*12, YBK*12a]. In the case of human skin, the hyperspectral modeling of skin appearance attributes provides a myriad of creative opportunities not only for aesthetic and entertainment applications, but also for educational and disease prevention projects. For example, it can be employed in IR skin imaging to enable the generation of unique images depicting an "ethereal" skin appearance often explored in artistic works [San09]. It can also be employed in UV skin imaging to enhance the appearance of photodamage effects (*e.g.*, the clumping of melanin) [MK66, Ful97], thus contributing to increase the willingness of individuals to adopt UV protection measures that can reduce skin cancer risk [SGG*09]. In addition, hyperspectral skin responses can be employed in non-invasive health-monitoring procedures of use to medical and cosmetics research as well as clinical practice. For example, UV responses can be used in the assessment of the intrinsic photoprotective properties of a skin specimen [NZS*06], while IR responses can be used in the assessment of skin hydration [APS*02], a key factor contributing to skin health.

In this paper, we present the first hyperspectral skin appearance model, henceforth referred to as HyLIoS (*Hy*perspectral *L*ight *I*mpingement *o*n *S*kin), that predictively simulates the light-attenuation processes that take place within the skin tissues in order to determine the spectral responses of this complex biological material in the UV, visible and IR domains. The first principles approach used in its design takes into account not only the detailed layered structure of the skin tissues, but also the particle nature of its main light-attenuation agents, namely the melanosomes (spheroidal melanin-containing organelles [AHC*01]). Within this modeling framework, the melanosomes' size, shape, orientation and distribution are probabilistically incorporated into the light transport simulations that also take into account the hyperspectral absorption and scattering properties of the remaining light-attenuation agents occurring in each layer. The proposed model employs an algorithmic formulation that allows for its straightforward integration into image synthesis pipelines. The correctness of its predictions are quantitatively and qualitatively evaluated through comparisons with actual measured data (from 250 nm to 2500 nm) reported in the scientific literature. In addition, images rendered using the HyLIoS model are employed to further illustrate its predictive capabilities and its use in hyperspectral skin imaging systems.

2 Related Work

In this section, we briefly review key developments on the modeling of skin appearance within the computer graphics field. The reader interested in a more detailed examination of this body of work is referred to comprehensive texts on this topic [DRS07, INN07, BK10].

Skin appearance models employed in realistic image synthesis can be roughly categorized into two groups: deterministic and non-nondeterministic. Deterministic models (*e.g.*, [DJ06, WMP*06,

dLE07, JSG09]) simulate the light and skin interactions using formulations based on analytical approximations to the radiative transfer equation such as the Kubelka-Munk theory, the diffusion theory [INN07, BK10] and the discrete-ordinate approximation [Sta01]. Non-deterministic models (*e.g.*, [HK93, NL01, KB04] simulate these interactions using stochastic techniques based on Monte Carlo methods [INN07,BK10]. While deterministic models are amenable to analytical manipulation, non-deterministic models offer more flexibility, albeit at a greater computational cost.

To date, these modeling efforts have been aimed at applications in the visible domain, *i.e.*, the existing skin appearance models are not designed for providing predictive spectral responses with respect to a broader spectral domain, from UV to IR. For instance, as stated by Anderson and Parish [AP82], the effects of melanin on skin color and UV light attenuation must be related not only to melanin content, but also to where it is found and how it is dispersed within the cutaneous tissues. Although all existing skin appearance models account for the presence of melanin, none of them accounts for the particle nature and distribution of melanosomes within the different epidermal layers. In addition, to the best of our knowledge, the existing models do not take into account in their formulations the presence and distribution of other major contributors to light attenuation outside the visible domain such as keratin, DNA, urocanic acid, water and lipids [You97, MTY09].

Besides the modeling efforts highlighted above, there have also been relevant computer graphics works involving the measurement of skin spectral responses and the capture of skin appearance data (*e.g.*, [MWL*99a, FBLS05, WMP*06, DWd*08, GHP*08]). It is worth noting that these efforts were also aimed at applications in the visible domain. Consequently, they primarily target the acquisition of skin appearance data in this domain. Outside the computer graphics field, a number of research groups are working on the measurement of skin topographical data using infrared-based sensors (*e.g.*, [HASS10]).

3 Biophysical Background

In order to predictively model the appearance attributes of human skin, it is necessary to account for its intrinsic optical properties, which control its interactions with light. Although previous works in this area have examined these properties, for completeness, we briefly review them from a hyperspectral perspective in this section.

Skin is usually described as being composed of three main tissues, namely stratum corneum, epidermis and dermis [MTY09]. The stratum corneum and the epidermal layers (stratum lucidum, stratum granulosum, stratum spinosum and stratum basale) are composed of stratified cells, and their combined thickness is about one millimeter [AP82, dG95]. The stratum lucidum is a clear layer found in thicker skin region such as palms and soles [dG95]. The dermis forms the bulk of the full thickness of skin. It can be divided into the papillary dermis and reticular dermis, with a combined thickness that may reach up to four millimeters [AP82]. Compared to the reticular dermis, the papillary dermis is relatively thin and contains smaller-sized structural fibers. The dermis also contains a network of blood vessels, with wider vessels being located in the reticular dermis.

Light impinging on the skin surface can be reflected back to the environment or transmitted to its internal tissues, a process that can be described in terms of the Fresnel equations [AP82]. In the remainder of this section, we outline the most important materials that contribute to the attenuation (absorption and scattering) of light travelling within the cutaneous tissues in the UV, visible and IR domains.

3.1 Light-Absorbing Materials

Relevant light-absorbing materials acting in the UV domain are situated within the stratum corneum and epidermis [You97]. These include DNA, keratin, urocanic acid and melanin, which may occur in two forms within human skin: the brown-black eumelanins and the yellow-red pheomelanins [Che95]. The absorption spectra of these pigments are plotted in Figure 2 (top row).

Melanin is also a significant absorber in the visible range [AP82]. It is synthesized by melanocyte cells in the stratum basale, where it is preferentially concentrated [dG95, AP82]. As the epidermal cells move upward, it is distributed throughout the full thickness of the upper layers [KSZC91]. Although melanin may occur in a degraded or colloidal form known as melanin "dust" [Pat95], it is predominantly found within the melanosomes, with its content within an individual melanosome ranging from 17.9% to 72.3% [KSZC91].

Blood-borne pigments, such as oxyhemoglobin, deoxyhemoglobin, carboxyhemoglobin, methemoglobin, sulfhemoglobin, bilirubin and beta-carotene, found in the dermis are also relevant absorbers in the UV and visible domains [JHM*55b, BCK*12]. It is worth noting that beta-carotene may be also found in the epidermis and stratum corneum [AP82]. The absorption spectra of these pigments are plotted in Figure 2 (center row and bottom left).

Water and lipids found throughout the skin dominate the absorption of light in the IR domain [JHM*55a, CA13], notably within the thick dermis [MTY09]. Their prominent contributions are accentuated beyond 1100 nm [AP82]. The absorption spectra of these materials are plotted in Figure 2 (bottom right).

3.2 Light-Scattering Materials

Light is mostly scattered by heterogeneous structures within the skin tissues such as cells, organelles and fibers [AP82, KSZC91]. Among these structures, the melanosomes have a central role in the attenuation of light travelling within human skin, notably in the UV and visible spectral domains. Accordingly, melanin-laden melanosomes that absorb and scatter UV radiation represent the most important intrinsic photoprotective mechanism found in human skin [Pat95].

Typically, the volume fraction of the epidermis occupied by melanosomes varies from 1% (for lightly pigmented specimens) to 10% (for darkly pigmented specimens) [Lis13]. The melanosomes can be characterized as particles with the shape of a prolate spheroid whose dimensions are given in terms of their major and minor axes [AHC*01]. Their size is also directly proportional to the level of melanin pigmentation, on average varying from 0.40 $\mu m \times 0.17$ μm for lightly pigmented specimens to 0.69 $\mu m \times 0.28$ μm for darkly pigmented specimens [OGE73].

In lightly pigmented specimens, the melanosomes occur in groups surrounded by a transparent membrane forming melanin complexes or aggregates [SGPF69, OGE73], which are characterized to be approximately spherical in shape [SGPF69,KSZC91] (Figure 3). In darkly pigmented specimens, however, they occur as denser and individually dispersed particles [SGPF69,OGE73] (Figure 3). The melanosomes predominantly scatter light in the forward direction [Che95], which is consistent with the experimental investigations reporting that the epidermis, as a whole, has a forward scattering behavior [BVDL84].

The turbid dermal layers contain dense connective tissue. Light that penetrates into these layers are subject to Rayleigh scattering, which may be caused by the presence of small scale features, such as collagen fibers and fibrils, in the papillary dermis [AP82, Jac96]. Moreover, as light penetrates deeper into the dermal layers, it becomes progressively more diffuse [JAP87]. Eventually, the light traversing the dermis may reach the hypodermis. This adipose tissue consists mostly of cells

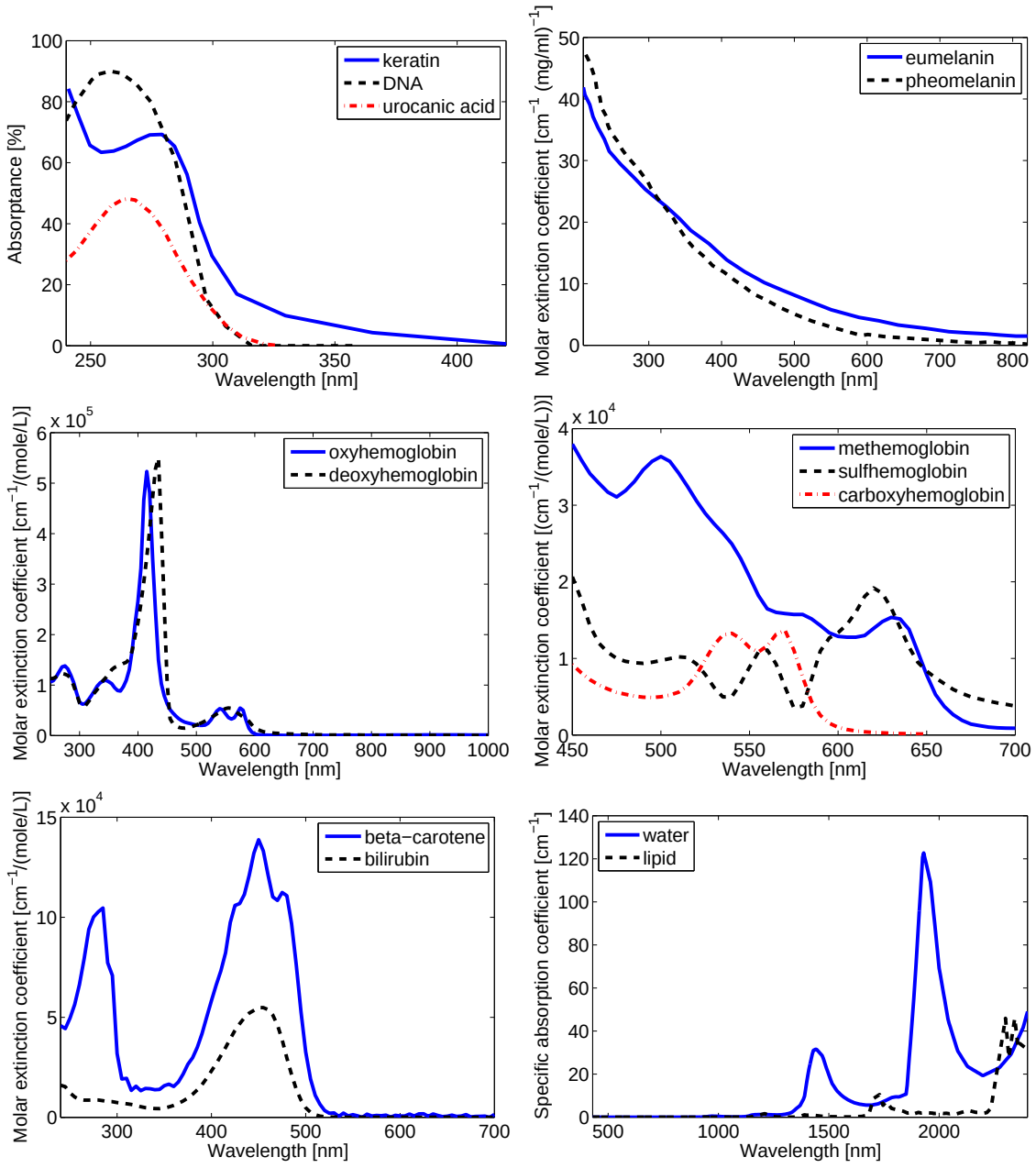

Figure 2: (Top left) Percent absorptance of solid keratin over a distance of 4 μm [BR61] and percent absorptance of 50 $\mu g/mL$ of DNA and 15 $\mu mol/L$ of urocanic acid over a distance of 1 cm [SG81, You97, Cle02, Oud12]. (Top right) Molar extinction coefficient of melanin [Jac01]. (Center left) Molar extinction coefficient of functional hemoglobins [Pra99]. (Center right) Molar extinction coefficient of dysfunctional hemoglobins [RBD*04,SANPR72,YB06]. (Bottom left) Molar extinction coefficient of beta-carotene and bilirubin [Pra01]. (Bottom right) Specific absorption coefficient of water [PW74, PF97] and lipid [AAM03, Pra04, vVSP*04].

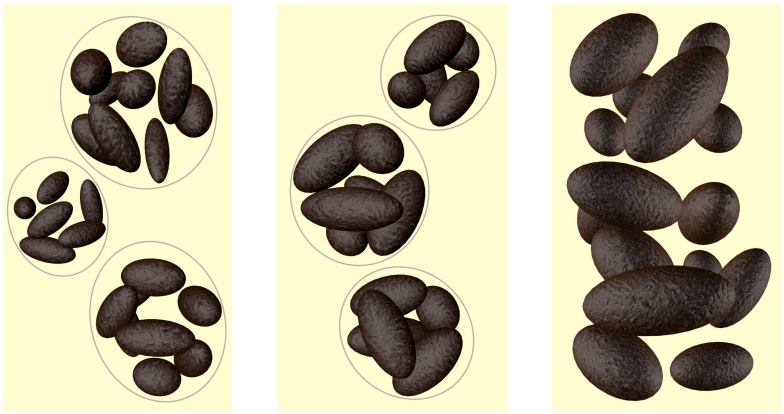

Figure 3: Sketches depicting the distribution of melanosomes within the epidermal layers of skin specimens with different levels of melanin pigmentation. Left: melanosome complexes found in lightly pigmented specimens. Center: more compact melanosome complexes found in moderately pigmented specimens. Right: individually dispersed melanosomes found in darkly pigmented specimens.

containing a number of smooth droplets of lipids whose size is larger than that of typical tissue scatterers [MTY09]. Nonetheless, light remission by large cellular structures in the hypodermis can further contribute to increase the scattering of light within the dermis [MTY09].

4 The HyLIoS Model

The proposed model employs stochastic techniques to simulate the interactions of light with the main cutaneous tissues, namely stratum corneum, stratum granulosum, stratum spinosum, stratum basale, papillary dermis and reticular dermis. Each of these tissues is represented by a layer modeled as a semi-infinite slab as illustrated in Figure 4. These layers are defined by their thickness, refractive index and the presence of light-absorbing and scattering materials.

The propagation and attenuation of light within the various skin layers are simulated through an iterative random walk algorithm which is schematically presented in Figure 5. Within this simulation framework, absorbers represent materials that primarily absorb light, while attenuators represent materials that primarily scatter light as well as materials that significantly contribute to both absorption and scattering of light. Although light is represented by discrete rays, each one travelling at a given wavelength λ, the attenuation events are probabilistically accounted for using ray optics as well as waves optics resources when appropriate.

At the start of each iteration, a Fresnel test [BK10] is performed when a ray hits a layer interface. If the ray exits the skin, a reflection or transmission event is recorded, and the iteration is terminated. Otherwise, the distance until the next attenuation event is probabilistically computed using the spectral attenuation coefficients, denoted by $\mu(\lambda)$, associated with the absorbers and attenuators present in the layer being traversed by the ray. More specifically, for each $\mu(\lambda)$, the

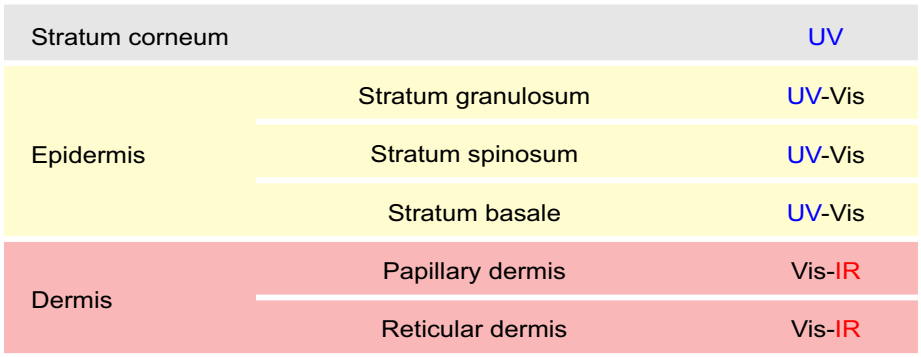

Figure 4: Diagram showing the main skin layers modeled by the proposed hyperspectral skin appearance model. The main light-absorbing spectral domains associated with each layer are identified as UV (ultraviolet), Vis (visible) and IR (infrared). The icons on the left denote the main scattering materials associated with a given layer, namely (from top to bottom) cellular structures, melanosomes and connective fibers.

corresponding distance [KB07] is given by:

$$d(\lambda) = -\frac{1}{\mu(\lambda)} \ln \xi, \tag{1}$$

where ξ is a random number uniformly sampled from $[0, 1)$. The smallest value of $d(\lambda)$ computed for all attenuation coefficients is set as the distance to the next attenuation event, *i.e.*, the ray is advanced this minimum distance.

If the ray hits a layer interface, the process reiterates from the Fresnel test. Otherwise, the ray is absorbed or scattered. When a ray interacts with an attenuator, a probabilistic test is used to determine whether the ray is absorbed. If it is not absorbed, its direction of propagation is probabilistically perturbed accordingly. The distance until the next attenuation event is then generated (Equation 1), and the random walk proceeds. In the remainder of this section, we described how the light-attenuation contributions of absorbers, attenuators and large scale cellular structures are accounted for in the algorithmic formulation of the proposed model.

4.1 Absorbers

The spectral attenuation coefficient of an absorber is given by its spectral specific absorption coefficient denoted by $\zeta(\lambda)$. All absorbers mentioned in Section 3.1 are incorporated into the HyLIoS model. These specific absorption coefficients may be incorporated into the model directly if their values are available. Otherwise, they are calculated using the spectral molar extinction coefficients, Υ, and molar weights, w, of the absorbers:

$$\zeta(\lambda) = \frac{\Upsilon(\lambda)}{w} \ln 10. \tag{2}$$

Note that the factor of $\ln 10$ is needed to convert from an absorbance value (molar extinction) to an specific absorption coefficient.

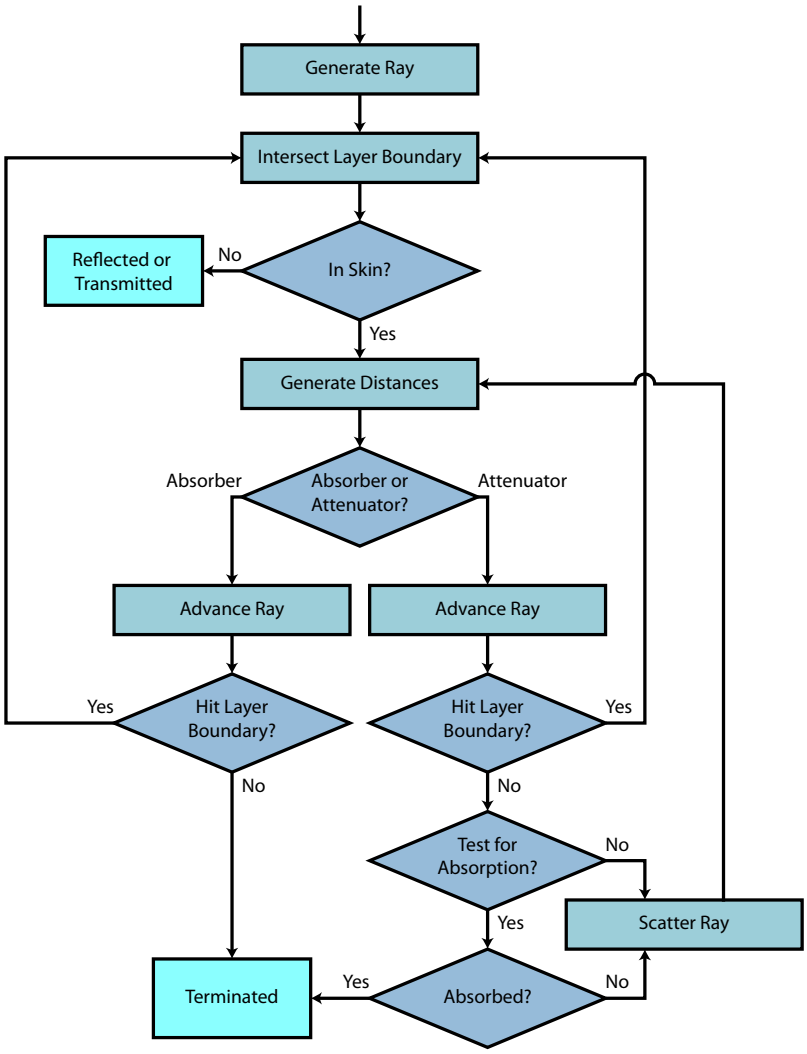

Figure 5: Flowchart depicting the general structure of the iterative random walk algorithm employed by the proposed skin appearance model.

For DNA and urocanic acid, additional data is required. Specifically, we need their density and molar mass, respectively, in skin. From the literature, the molar mass of urocanic acid in stratum corneum ranges from 0.0029 mol/L to 0.0287 mol/L [OWT*97], and we use a value of 0.01 mol/L. For DNA, the mass per cell is approximately 6.4E-12 g [Var01], and there are approximately 1.1E11 cells [Fli06] in skin. The volume of skin is 3.8 L [AH04]. Thus, the density of DNA in skin is approximately 0.185 g/L.

In order to account for the contributions of all absorbers present in a given layer, we compute the spectral volumetric absorption coefficient given by the weighted sum of their specific absorption coefficients. For example, the absorption in the papillary dermis is primarily due to water, lipids and blood pigments. Let the blood borne pigments oxyhemoglobin, deoxyhemoglobin, carboxyhemoglobin, methemoglobin, sulfhemoglobin, beta-carotene and bilirubin be denoted by oh, dh, ch, mh, sh, bc and bil, respectively. The corresponding volumetric absorption coefficient of the papillary dermis can then be calculated as:

$$\begin{aligned}\mu_a^p(\lambda) =&\zeta_{water}(\lambda)v^p_{water} + \zeta_{lipids}(\lambda)v^p_{lipids} + (\zeta_{oh}(\lambda)v^b_{oh} + \zeta_{dh}(\lambda)v^b_{dh} \\ &+\zeta_{ch}(\lambda)v^b_{sh} + \zeta_{mh}(\lambda)v^b_{mh} + \zeta_{sh}(\lambda)v^b_{sh} + \zeta_{bc}(\lambda)v^b_{bc} + \zeta_{bil}(\lambda)v^b_{bil})v^p_{blood},\end{aligned} \tag{3}$$

where ζ_i, v_i^p and v_i^b correspond to the specific absorption coefficient of a given absorber i, its volume fraction with respect to the papillary dermis, and its volume fraction with respect to whole blood, respectively.

Recall that melanin may be found dispersed in a colloidal form or within the melanosomes (Section 3.1). For the former case, its specific absorption coefficients (for eumelanin and pheomelanin) are aggregated to the specific absorption coefficients of the pigments found in a given layer as described earlier. For the latter case, the computation of its attenuation coefficient takes into account its concentration within each individual melanosome, and the attenuation testing is performed considering the geometrical and optical characteristics of each melanin-containing melanosome as further examined in Section 4.2.2.

4.2 Attenuators

Connective fibers and melanosomes are incorporated into the proposed model as attenuators. Based on experimental investigations [Lat84], the perturbations caused by these materials on the propagated light is assumed to be azimuthally symmetric. Accordingly, the corresponding azimuthal angle of perturbation is uniformly sampled from $[0, 2\pi)$.

4.2.1 Connective Fibres

The scattering caused by the thin connective fibers in the papillary dermis is assumed to follow the Rayleigh scattering formulation [Jac96]. Hence, the corresponding attenuation coefficient is given by the Rayleigh scattering coefficient, which is calculated using the following expression [McC76]:

$$\mu_s^R(\lambda) = \frac{128\pi^5 r^6 D}{3\lambda^4}\left(\frac{\eta^2-1}{\eta^2+1}\right)^2, \tag{4}$$

where r and D represent the radius and density of the scatterer, respectively, and η corresponds to the ratio between the refractive index of the scatter to the refractive index of its surrounding

medium. In our simulations, we consider the following values for these parameters [Jac96]: $r = 100\ nm$, $\eta = 1.55/1.33$, and D given by the following formula:

$$D = 0.22\left(\frac{4}{3}\pi r^3\right)^{-1}. \tag{5}$$

The ray direction of propagation is perturbed employing the Rayleigh scattering distribution. Accordingly, the polar angle θ_R is generated using Algorithm 1, where ξ_1 and ξ_2 are random numbers uniformly sampled from $[0, 1)$. Since the attenuation coefficient computed for these materials describes bulk scattering, the contributions of these attenuators are taken into account only once per ray pass through the papillary dermis.

Algorithm 1 Rayleigh perturbation

repeat
  $\theta_R = \pi\xi_1$
until $\xi_2 \leq \left(\frac{3\sqrt{6}}{8}\right)(1 + \cos^2\theta_R)\sin\theta_R$
return θ_R

4.2.2 Melanosomes and Melanosome Complexes

The proposed model accounts for the scattering and absorption of light by individually dispersed melanosomes (in darkly pigment specimens) and by melanosome complexes (in lightly and moderately pigmented specimens). Melanosomes are modeled as prolate spheroids employing average dimensions reported in the literature (Section 3.2), while melanosome complexes are modeled as spheres [KSZC91]. Based on experimental observations [SGPF69], for lightly pigmented specimens, the sphere diameter is set to be twice the major axis of the spheroids representing the encapsulated melanosomes. Similarly, for moderately pigmented specimens, this diameter is set to be equal to the major axis of the spheroids [SGPF69].

The attenuation coefficient of a melanosome is given by its geometric attenuation coefficient [KB07]:

$$\mu_g = \frac{S}{V}\frac{v}{4}, \tag{6}$$

where S is the surface area, V is the volume and v is the volume fraction. The ratio S/V is calculated as:

$$\begin{aligned} \frac{S}{V} &= \frac{3}{2a}\left(\frac{a}{c} + \frac{\arcsin b}{b}\right), \\ b &= \sqrt{1 - \frac{a^2}{c^2}}. \end{aligned} \tag{7}$$

In the equation above, a and c correspond to the lengths of the semi-minor and semi-major axes, respectively.

Once the distance d is computed, by plugging μ_g into Equation 1, the orientation of the spheroid is selected by sampling the probability distribution function (PDF) associated with the orientations that were considered while generating the distance. This PDF [YBK*12b] is given by:

$$P_m(\alpha, \beta) = \left(\frac{\chi_1(1 - |\cos\alpha|) + \chi_2|\cos\alpha|}{\chi_1 + \chi_2}, \frac{1}{2\pi}\right), \tag{8}$$

where α and β correspond respectively to the polar and azimuthal angles defining the ray direction, and χ_1 and χ_2 correspond to the cross-sectional areas of the spheroid associated with its minor and major axes, respectively. Finally, the hitting point on the spheroid surface is randomly selected among the set of points facing the ray.

After the position, orientation and hitting point are selected, the model simulates the light-melanosome interactions as described next. A ray travelling within the melanosome is tested for absorption employing Equation 1 and the aggregated specific absorption coefficients of eumelanin and pheomelanin as the corresponding attenuation coefficient (Section 4.1). If not absorbed, the ray may bounce inside the spheroid due to refractive index differences between melanin and the surrounding medium (epidermal tissue), or it may be transmitted out of the spheroid. When the ray is bounced, it is diffusely perturbed to account for the melanosome's irregular morphology [KSZC91], *i.e.*, the polar perturbation angle is sampled from $[0, \pi/2)$ using a PDF based on a cosine distribution [BK10].

In the case of the melanosome complexes, their attenuation coefficient is also obtained using Equation 6 with the ratio S/V given by $3/r_s$ [KB07], where r_s is the radius of the corresponding sphere. When a ray encounters a melanosome complex, it interacts with at most m encapsulated melanosomes, where m is the ratio of the diameter of the encapsulating sphere to the minor axis of the spheroid representing the melanosomes [SGPF69]. Each of these interactions will involve the melanosome orientation selection and the absorption testing described above.

If a ray is not absorbed by an individually dispersed melanosome or a melanosome complex, it is scattered. The forward scattering behavior of a melanosome [Che95] is simulated using a experimentally-based procedure. More specifically, the corresponding polar scattering angle θ_m is sampled from an exponential distribution that has a mean angle $\theta_\circ$. This mean angle was selected to be 5° based on wave optics experimental observations on the scattering behavior of biological organelles [Lat84]. Furthermore, since light-melanosome interactions have an increasingly diminished contribution in the near IR (from 780 nm to 1400 nm), being essentially negligible beyond ~ 1100 nm [AP82], we linearly reduce $\theta_\circ$ to 0 over this region. Accordingly, the polar angle θ_m is generated using Algorithm 2, where ξ_3 and ξ_4 are random numbers uniformly sampled from $[0, 1)$. The same algorithm is employed for a melanosome complex, *i.e.*, after the last encapsulated melanosome is tested for absorption, Algorithm 2 is applied.

Algorithm 2 Exponential perturbation (mean angle $\theta_\circ$)

$\phi = \arctan(\theta_\circ)$
$max = 1/\theta_\circ \times \exp(-\phi/\theta_\circ) \times \sin(\phi)$
repeat
  $\theta_m = \pi\xi_3$
until $max \times \xi_4 \leq 1/\theta_\circ \times \exp(-\theta_m/\theta_\circ) \times \sin(\theta_m)$
return θ_m

4.3 Large Scale Cellular Structures

A portion of the light that interacts with the stratum corneum cells may be reflected back to the environment following the execution of a Fresnel test [AP82]. To account for the influence of the skin surface roughness on the distribution of the reflected rays, the surface normals are perturbed using a formula based on the Trowbridge-Reitz function [BK10], which represents rough air-cell interfaces using randomly-curved microareas. Accordingly, when a ray impinges on the skin

surface, the azimuthal angle of the perturbed surface normal is uniformly sampled from $[0, 2\pi)$, while the polar angle θ_s is generated using the following distribution:

$$P_s(\theta_s) = \frac{s^4}{(s^2 \cos^2 \theta_s + \sin^2 \theta_s)^2} \sin \theta_s,$$

where s is the roughness parameter associated with the aspect ratio of the stratum corneum cells, *i.e.*, the flatter the cells (higher s), the closer the spatial distribution of reflected rays approaches a specular distribution.

Since the large cellular structures in the hypodermis reflect most of the light impinging on it (Section 3.2), the dermal-hypodermal junction is set to have a reflectance equal to 1. In addition, considering that light becomes progressively more diffuse as it travels further within the dermis [JAP87], the rays reflected at the dermal-hypodermal junction are diffusely perturbed, *i.e.*, the azimuthal perturbation angle is uniformly sampled from $[0, 2\pi)$ and the polar perturbation angle is sampled from $[0, \pi/2)$ using a PDF based on a cosine distribution [BK10].

5 Results and Discussion

In order to evaluate the correctness and predictive capabilities of the proposed model, we have compared modeled results with measured data and experimental observations reported in the scientific literature. In the absence of measured skin characterization data for the specimens used in the actual experiments, the values for pigmentation parameters used to generate the modeled curves (Tables 1 and 2, and Figure 6) were selected based on the specimens' description and the corresponding ranges for these parameters also provided in the scientific literature. Also note that in the model, the axes of the melanosomes for the stratum spinosum and stratum granulosum were set to be 50% and 25% of the values in Table 1, respectively, to account for melanosome degradation in these upper epidermal layers [NZS*06]. Note that most of the biophysical quantities employed in the simulations, such as refractive indices and absorption coefficients, are not normally subject to change, and, therefore, can be kept fixed during the simulations.

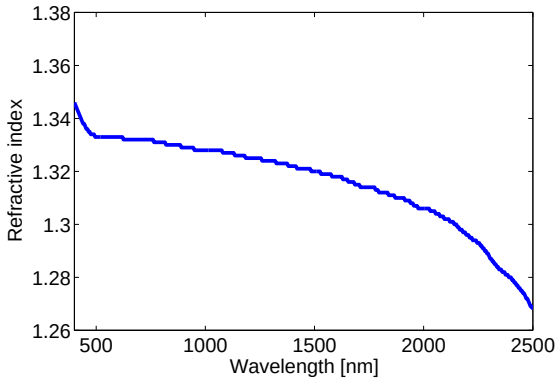

Figure 6: Refractive index of water [PW74].

Existing skin appearance models designed for applications in the visible domain, such as the diffusion theory based model proposed by Donner and Jensen [DJ06] (henceforth referred to as

Parameter	S1	S2	S3	S4	Source
Surface Fold Aspect Ratio	0.1	0.25	0.1	0.45	[TKK*01, MTKLL*02]
Stratum Corneum Thickness (cm)	0.001	0.001	0.0004	0.0002	[Dif80, AP82]
Stratum Granulosum Thickness (cm)	0.0017	0.0033	0.0033	0.0007	[RR10]
Stratum Spinosum Thickness (cm)	0.0017	0.0033	0.0033	0.0007	[RR10]
Stratum Basale Thickness (cm)	0.0017	0.0033	0.0033	0.0007	[Shi07]
Papillary Dermis Thickness (cm)	0.02	0.01	0.02	0.023	[AP81]
Reticular Dermis Thickness (cm)	0.1	0.1	0.125	0.2	[AP81]
Stratum Granulosum Melanosome Content (%)	1.0	0.0	0.0	10.0	[KSZC91, Lis13]
Stratum Spinosum Melanosome Content (%)	1.0	0.0	0.0	10.0	[KSZC91, Lis13]
Stratum Basale Melanosome Content (%)	1.0	3.75	3.0	10.0	[KSZC91, Lis13]
Stratum Granulosum Colloidal Melanin Content (%)	0.8	1.25	1.35	15.0	[AAB*02, KSZC91, Pat95]
Stratum Spinosum Colloidal Melanin Content (%)	0.8	1.25	1.35	15.0	[AAB*02, KSZC91, Pat95]
Stratum Basale Colloidal Melanin Content (%)	0.8	1.25	1.35	15.0	[AAB*02, KSZC91, Pat95]
Melanosome Eumelanin Concentration (mg/mL)	90.0	50.0	32.0	50.0	[THW*91, HOD*05]
Melanosome Pheomelanin Concentration (mg/mL)	4.0	2.0	2.0	4.0	[THW*91, HOD*05]
Melanosome Dimensions ($\mu m \times \mu m$)	0.41×0.17	0.41×0.17	0.41×0.17	0.69×0.28	[OGE73]
Papillary Dermis Blood Content (%)	0.2	0.7	0.3	2.5	[Fle00, Jac96]
Reticular Dermis Blood Content (%)	0.2	0.7	0.3	2.5	[Fle00, Jac96]
Oxygenated Blood Fraction (%)	75.0	95.0	75.0	75.0	[Ang01]

Table 1: Four sets of HyLIoS parameters employed to characterize the distinct skin specimens considered in the quantitative comparisons presented in this work. Note that in the absence of measured skin characterization data for the specimens used in the actual experiments, the values assigned to the pigmentation parameters employed in the computation of the modeled curves were selected based on the specimens' descriptions reported in the documents describing the actual experiments and the corresponding ranges for these parameters provided in the scientific literature. Accordingly, the datasets S1, S2 and S3 correspond to individuals with relative low level of melanin pigmentation [VGI94, CA13], while dataset S4 corresponds to an individual with a high level of melanin pigmentation [JHM*55a, JHM*55b].

Parameter	Value	Source
Stratum Corneum Refractive Index	1.55	[TBS*95, Dif83]
Epidermis Refractive Index	1.4	[TBS*95, ToPoIE07]
Papillary Dermis Refractive Index	1.39	[TBS*95, JAP87]
Reticular Dermis Refractive Index	1.41	[TBS*95, JAP87]
Melanin Refractive Index	1.7	[BGK*00]
Hemoglobin Concentration in Whole Blood (mg/mL)	147.0	[LHGC99, Fle00]
Methemoglobin Concentration in Whole Blood (mg/mL)	1.5	[Hay05]
Carboxyhemoglobin Concentration in Whole Blood (mg/mL)	1.5	[CKW*04]
Sulfhemoglobin Concentration in Whole Blood (mg/mL)	0.0	[YB06]
Whole Blood Bilirubin Concentration (mg/mL)	0.003	[ZHS04]
Stratum Corneum Beta-carotene Concentration (mg/mL)	2.1E-4	[LMRPP75]
Epidermis Beta-carotene Concentration (mg/mL)	2.1E-4	[LMRPP75]
Blood Beta-carotene Concentration (mg/mL)	7.0E-5	[LMRPP75]
Stratum Corneum Water Content (%)	35.0	[AH04, NMS10]
Epidermis Water Content (%)	60.0	[AH04, VKS*04]
Papillary Dermis Water Content (%)	75.0	[AH04, VKS*04]
Reticular Dermis Water Content (%)	75.0	[AH04, VKS*04]
Stratum Corneum Lipid Content (%)	35.0	[WHH88]
Epidermis Lipid Content (%)	20.0	[SCW91, CBB*01, AH04]
Papillary Dermis Lipid Content (%)	15.1	[SCW91, CBB*01, AH04]
Reticular Dermis Lipid Content (%)	17.33	[SCW91, CBB*01, AH04]
Stratum Corneum Keratin Content (%)	65.0	[Fuc95, Shi07, Gaw02]
Stratum Corneum Urocanic Acid Density (mol/L)	0.01	[You97]
Skin DNA Density (mg/mL)	0.185	[Var01, AH04, Fli06]

Table 2: Set of HyLIoS parameters kept fixed for the simulations that resulted in the modeled curves depicted in quantitative comparisons presented in this work. The refractive indices for the skin layers were measured at 1300 nm as reported in the listed sources.

DJ06) and the Monte Carlo based proposed by Krishnaswamy and Baranoski [KB04] (known as BioSpec), assume melanin to be uniformly distributed in a single layer representing epidermis. Moreover, they do not take into account either the particle nature or the distribution patterns of the melanosomes (Section 3.2). These limitations preclude these models from accounting for detour and sieve effects, which can lead to prominent discrepancies, notably in the blue-end of spectrum characterized by higher melanin absorption. Such discrepancies can be observed in the graphs presented in Figure 7. These graphs show comparisons of modeled results provided by DJ06, BioSpec and HyLIoS with measured results provided by Vrhel et al. [VGI94] considering an angle of incidence of 45°, which are made available in a spectra database at the North Carolina State University (NCSU). In these comparisons, we employed NCSU curves used as references in the original evaluations of DJ06 and BioSpec. Note that the DJ06 modeled results depicted in Figure 7 were originally computed with the amount of eumelanin set to zero as reported by Donner and Jensen [DJ06]. Although this can mitigate the absorption related limitations of the diffusion theory approximation outlined in Section 2, we remark that eumelanin is the dominant form of melanin present in human skin under normal physiological conditions [AP82, Che95, HOD*05, KSZC91].

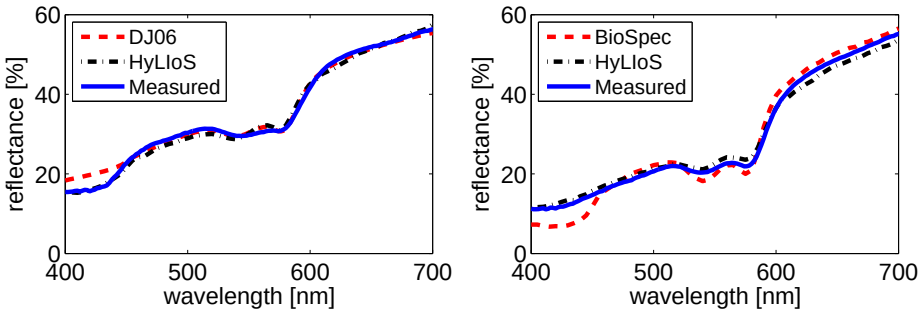

Figure 7: Comparisons of modeled spectral curves obtained using DJ06 [DJ06], BioSpec [BK10] and HyLIoS models with measured NCSU spectral curves 117 (left) and 113 (right) [VGI94]. The HyLIoS curves on the left and right were computed using the pigmentation datasets S1 and S2, respectively (Tables 1 and 2).

The first principles simulation approach employed by HyLIoS accounts not only for detour and sieve effects, but also for the strong forward scattering behavior of the epidermal layers, notably in the UV domain [BVDL84] as shown in the plot presented in Figure 8. Recall that the particle nature and distribution patterns of the melanosomes have an even stronger influence on the skin spectral responses in the UV range [AP82, Che95], and the existing spectral models, different from HyLIoS, do not account for these factors. Hence, the simple incorporation of additional absorbers acting in the UV domain into these models would likely lead to discrepancies similar to those observed in the blue-end of the visible spectrum (Figure 7).

In order to demonstrate the predictive capabilities of HyLIoS across the UV-Visible-IR range, we compared modeled curves with measured curves provided by Cooksey and Allen [CA13] and Jacquez et al. [JHM*55a, JHM*55b], which were obtained for lightly and darkly pigmented skin specimens considering angles of incidence of 8° and 16.75°, respectively. As it can be observed in the graphs provided in Figure 9, the relevant hyperspectral features (represented by the "peaks" and "valleys") and trends are reproduced by the modeled curves. For example, for wavelengths

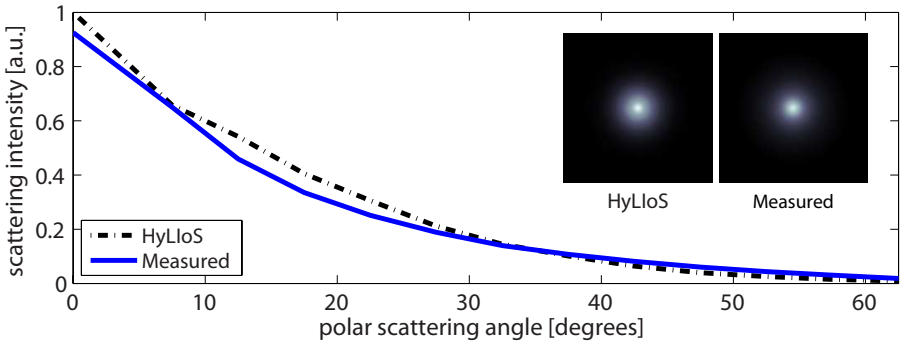

Figure 8: Comparison of modeled subsurface scattering data obtained using HyLIoS with measured subsurface scattering data provided by Bruls and van der Leun [BVDL84] for the epidermis of a lightly pigmented skin specimen considering normal incidence of UV light (at 302 nm). The modeled data was computed using the pigmentation dataset S2 (Tables 1 and 2). The insets depict orthographic projections of the measured and modeled subsurface scattering data presented in the graph.

longer than $\approx$ 1300 nm, the absorption is dominated by the presence of water and lipids instead of melanin pigmentation [AP82], resulting in a similarity between the measured reflectance spectra in this region. Such a similarity can also be observed between the modeled reflectance spectra. We note that localized quantitative variations can be expected across the UV-Visible-IR domains since we employed for both specimens the same average values for key characterization parameters such as the water content and the refractive index associated with each skin layer. As demonstrated by Cooksey and Allen [CA13], population variability is the most significant source of uncertainty in the measurement of skin reflectance. We note, however, that our modeled results were obtained using parameter values within physiologically valid ranges indicated in the scientific literature.

We also examined the predictions of HyLIoS with respect to the spatial distribution of light. Although these predictions can be represented in terms of BSSRDF (bidirectional scattering-surface reflectance distribution function), we quantified them in terms of BRDF (bidirectional reflectance distribution function) and integrated the resulting values over the visible domain to obtain BRDF curves that could be compared to measured BRDF curves provided by Marschner et at. [MWL*99b]. As it can be observed in the comparisons depicted in Figure 10, HyLIoS can capture the angular dependency of the spatial distribution of light interacting with human skin in the visible domain. Moreover, recall that IR light can penetrate deeper into the cutaneous tissues than UV light [AP82], and it can reach the dermal layers where it becomes progressively more diffuse [JAP87]. As a result, the subsurface reflectance has a more dominant role in the IR domain, and the overall reflected IR light, notably in the region below 1300 nm (less susceptible to water absorption), has a more diffuse distribution than UV light [AP82, HASS10]. The scattering plots presented in Figure 11 indicate that HyLIoS can capture these distinct spatial distribution patterns of UV and IR light interacting with human skin.

The presence of brownish spots (freckles) caused by the deposition or clumping of melanin is enhanced when a skin specimen is exposed to UV light [MK66,Ful97], and it is not detectable when the specimen is exposed to IR light [San09]. As depicted in the image of a light pigmented individual

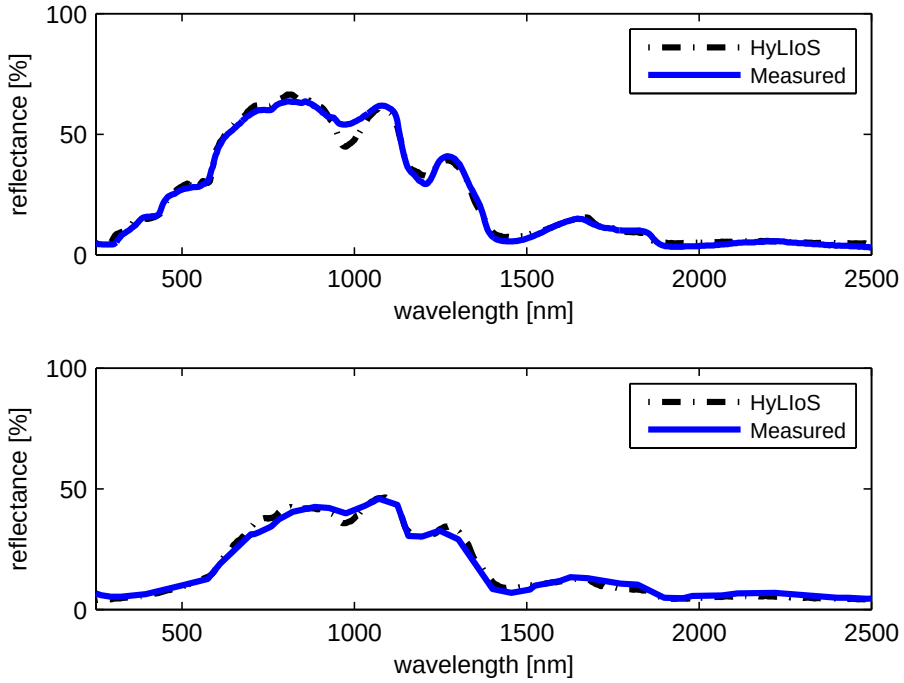

Figure 9: Comparisons of modeled hyperspectral curves obtained using HyLIoS with measured curves for a lightly pigmented specimen (top) provided by Cooksey and Allen [CA13] and a darkly pigmented specimen (bottom) provided by Jacquez *et al.* [JHM*55a, JHM*55b]. The HyLIoS curves (from 250 nm to 2500 nm) for the lightly and darkly pigmented specimens were computed using the pigmentation datasets S3 and S4, respectively (Tables 1 and 2).

presented in Figure 1, the proposed model can be used to predictively simulate these effects. More specifically, the subject's freckles are accentuated under exposure to UV light (Figure 1(*Left*)) and imperceptible under exposure to IR light (Figure 1(*Right*)). In addition, these images illustrate the distinct scattering behaviors observed in the UV and IR domains. For example, the subject shows a more diffuse light reflection behavior under exposure to IR light (Figure 1(*Right*)) than to UV light (Figure 1(*Left*)), which are consistent with observations reported in the scientific literature [AP82, HASS10]. Similarly, these distinct scattering behaviors can also be observed in the images presented in Figures 13(*Left*) and 14(*Left*).

As mentioned earlier, melanosomes packed with melanin are not only major contributors to the color of human skin, but also the most effective light-attenuation materials acting in UV domain [AP82, KSZC91, Che95]. Accordingly, an increase in epidermal melanin content leading to visible darker skin tones [AP82, Pat95], has its reductional effects on skin reflectance enhanced in the UV domain [MK66, Ful97]. These trends are qualitatively reproduced by the proposed model as illustrated by the images presented in Figures 12 and 13, respectively. Moreover, as it can be observed in these images, while an increase in epidermal melanin content from 7% to 30% results

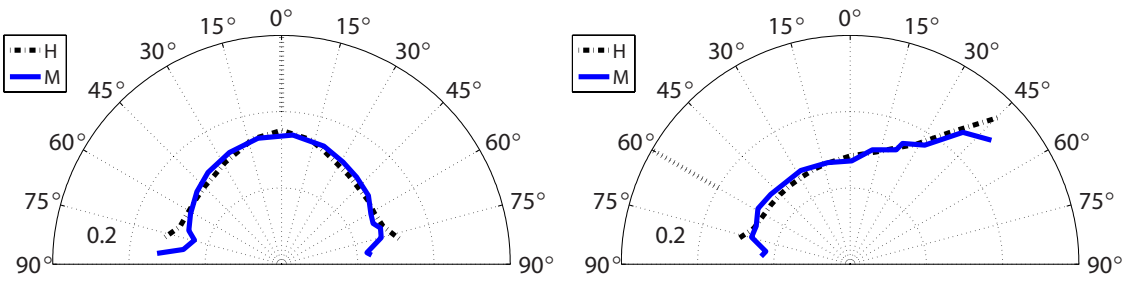

Figure 10: Comparison of modeled BRDF curves (H) provided by HyLIoS with measured BRDF curves (M) provided by Marschner et at. [MWL*99b] for a lightly pigmented specimen considering two angles of incidence: 0° (left) and 60° (right). The modeled curves were obtained considering the pigmentation dataset S1 (Tables 1 and 2).

in a darker skin appearance in the visible domain (Figure 12), such a change in appearance is negligible within the UV domain (Figure 13). This behavior is also consistent with measurements showing practically identical reflectance responses for moderately and darkly pigmented specimens in the UV domain [JHM*55b].

Within the IR domain, the skin spectral responses are primarily determined by the absorption bands of water [CA13, JHM*55a]. A myriad of physiological and environmental factors can alter the barrier function of skin thus intensifying water loss and leading to dehydration [APS*02]. A reduction of water content in the cutaneous tissues [Bla52], in turn, results in an increase in skin reflectance in the IR domain [APS*02]. As illustrated by the images presented in Figure 14, this qualitative behavior is also captured by the proposed model.

We remark that although the stochastic simulation approach employed by the HyLIoS model provides the flexibility and robustness required for the detailed modeling of the complex structural and optical characteristics of the cutaneous tissues, it incurs substantial computational costs. Accordingly, considering that it may take on the order of seconds (on a dual 6-core 2.66-GHz Intel Xeon machine) to obtain a hyperspectral reflectance curve for a given illumination and viewing geometry, it is fair to say that the current implementation of the HyLIoS model is not particularly suitable to real time applications that demand results on the order of milliseconds. Hence, to extend its use to this type of applications, it will be necessary to substantially reduce its computational costs through hardware and software acceleration mechanisms. For instance, several computational procedures employed by the proposed model can be performed offline, and their results stored and directly accessed during the image synthesis process.

6 Conclusion and Future Work

In this report, we have described the first hyperspectral skin appearance model presented in the computer graphics literature. It employs a first principles approach to simulate the light propagation and attenuation processes within the cutaneous tissues in the ultraviolet, visible and infrared domains. Its predictive capabilities have been evaluated through comparisons with actual measured data and further illustrated by rendered images depicting variations on skin appearance attributes consistent with experimental observations reported in the scientific literature.

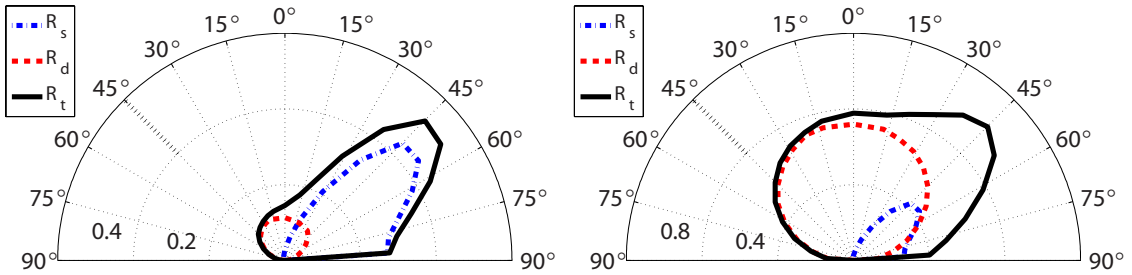

Figure 11: Scattering plots provided by HyLIoS showing surface (R_s), subsurface (R_d), and total (R_t) reflectance distributions in the UV (left) and IR (right) domains. Note the more diffuse total reflectance distribution of IR light (below 1300 nm) as reported in the scientific literature [AP82, HASS10]. These plots correspond to normalized bidirectional reflectance values at 365 nm (left) and 1100 nm (right) multiplied by the cosine of the reflection angle. The bidirectional reflectance values were computed considering an angle of incidence of 45° and using the pigmentation dataset S1 (Tables 1 and 2).

Besides its use in photo-realistic hyperspectral rendering frameworks, the proposed model can also be employed in hyperspectral visualization systems aimed at the investigation of adverse environmental factors affecting skin appearance, such as excessive UV exposure and water loss, and at the education of the general public with respect to the health risks posed by these factors. In order to foster interdisciplinary research collaborations in these areas, we intend to make the proposed model and the supporting biophysical data openly available for online use.

References

[AAB*02] Alaluf S., Atkins D., Barret K., Blount M., Carter N., Heath A.: Ethnic variation in melanin content and composition in photoexposed and photoprotected human skin. *Pigment Cell Research 15* (2002), 112–118.

[AAM03] Altshuler G. B., Anderson R. R., Manstein D.: Method and apparatus for the selective targeting of lipid-rich tissues. Patent, 8 2003.

[AH04] Agache P., Humbert P.: *Measuring the Skin.* Springer, 2004.

[AHC*01] Alaluf S., Heath A., Carter N., Atkins D., Mahalingam H., Barrett K., Kolb R., Smit N.: Variation in melanin content and composition in type V and type VI photoexposed and photoprotected human skin: the dominant role of DHI. *Pigment Cell Research 14* (2001), 337–347.

[Ang01] Angelopoulou E.: Understanding the color of human skin. In *Storage and Retrieval for Image and Video Databases* (2001).

[AP81] Anderson R. R., Parrish J. A.: The optics of human skin. *Invest Dermatol 77*, 1 (1981), 13–9.

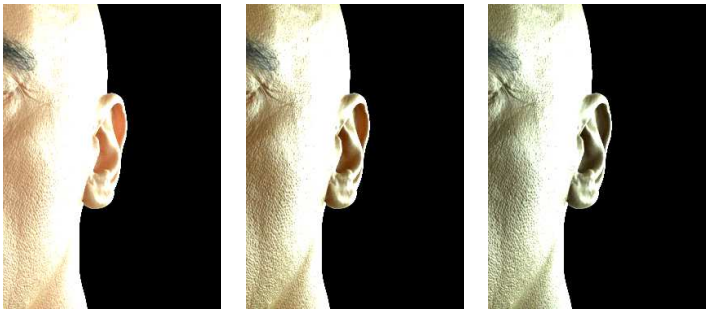

Figure 12: Images generated using the HyLIoS model to illustrate the effects of increased melanin pigmentation on the appearance attributes of human skin in the visible domain. Left: 1.5%. Middle: 7%. Right: 30%. Polygonal mesh courtesy of XYZ RGB Inc.

Figure 13: Images generated using the HyLIoS model to illustrate the reductional effects of increased melanin pigmentation on skin spectral responses in the UV domain. Left: 1.5%. Middle: 7%. Right: 30%. The UV responses (at 365 nm) are depicted in pseudo color. Polygonal mesh courtesy of XYZ RGB Inc.

Figure 14: Images generated using the HyLIoS model to illustrate the magnifying effects of dehydration on skin spectral responses in the IR domain. Dehydration was simulated by reducing the water content of the cutaneous tissues of a light pigmented specimen (1.5% epidermal melanin content) within physiological limits [Bla52] Left: No reduction. Middle: 20% reduction. Right: 40% reduction. The IR responses (at 1650 nm) are depicted in pseudo color. Polygonal mesh courtesy of XYZ RGB Inc.

[AP82] Anderson R., Parrish J.: Optical properties of human skin. In *The Science of Photomedicine* (N.Y., USA, 1982), Regan J., Parrish J., (Eds.), Plenun Press, pp. 147–194.

[APS*02] Attas M., Posthumus T., Schattka B., Sowa M., Mantsch H., Zhang S.: Long-wavelength near-infrared spectroscopic imaging for in-vivo sky hydration measurements. *Vibrational Spectroscopy 28* (2002), 37–43.

[BCK*12] Baranoski G. V. G., Chen T. F., Kimmel B. W., Miranda E., Yim D.: On the noninvasive optical monitoring and differentiation of methemoglobinemia and sulfhemoglobinemia. *J. of Biomed. Optics 17*, 9 (2012), 097005–1–14.

[BGK*00] Bashkatov A. N., Genina E. A., Kochubey V. I., Stolnitz M. M., Bashkatova T. A., Novikova O. V., Peshkova A. Y., Tuchin V. V.: Optical properties of melanin in the skin and skinlike phantoms. In *Controlling Tissue Optical Properties: Applications in Clinical Study* (2000), Tuchin V. V., (Ed.), vol. 4162, SPIE, pp. 219–226.

[BK10] Baranoski G. V. G., Krishnaswamy A.: *Light & Skin Interactions: Simulations for Computer Graphics Applications*. Morgan Kaufmann, 2010.

[Bla52] Blank I. H.: Factors which influence the water content of the stratum corneum1. *The Journal of Investigative Dermatology 18*, 6 (06 1952), 433–440.

[BR61] Bendit E. G., Ross D.: A technique for obtaining the ultraviolet absorption spectrum of solid keratin. *Applied Spectroscopy* (1961).

[BVDL84] Bruls W. A. G., Van Der Leun J. C.: Forward scattering properties of human epidermal layers. *Photochemistry and Photobiology 40*, 2 (1984), 231–242.

[CA13] Cooksey C., Allen D.: Reflectance measurements of human skin from the ultraviolet to the shortwave infrared (250 nm to 2500 nm). In *SPIE Vol. 8734, Active and Passive Signatures IV* (2013), Gilbreath G., Hawley C., (Eds.), pp. 87340N–1–9.

[CBB*01] Cerussi A. E., Berger A. J., Bevilacqua F., Shah N., Jakubowski D., Butler J., Holcombe R. F., Tromberg B. J.: Sources of absorption and scattering contrast for near-infrared optical mammography. *Academic radiology 8*, 3 (March 2001), 211–218.

[Che95] Chedekel M.: Photophysics and photochemistry of melanin. In *Melanin: Its Role in Human Photoprotection* (Overland Park, Kansas, USA, 1995), L. Zeise M. C., Fitzpatrick T., (Eds.), Valdenmar Publishing Co., pp. 11–22. 2223b.

[CKW*04] Cunnington A. J., Kendrick S. F. W., Wamola B., Lowe B., Newton C. R. J. C.: Carboxyhemoglobin levels in kenyan children with plasmodium falciparum malaria. *The American Journal of Tropical Medicine and Hygiene 71*, 1 (2004), 43–47.

[Cle02] Clendening B.: *UV Spectrophotometric Analysis of DNA and RNA*. Tech. rep., Hofstra University, 2002.

[CSB13] Cavalcanti P. G., Scharcanski J., Baranoski G. V.: A two-stage approach for discriminating melanocytic skin lesions using standard cameras. *Expert Systems with Applications 40*, 10 (2013), 4054–4064.

[dG95] de Graaff K. V.: *Human Anatomy*, 4th ed. Wm. C. Brown Publishers, Dubuque, IO, USA, 1995.

[Dif80] Diffey B. L.: Ultraviolet radiation physics and the skin. *Physics in Medicine and Biology 25*, 3 (1980), 405.

[Dif83] Diffey B.: A mathematical model for ultraviolet optics in skin. *Physics in Medicine and Biology 28*, 6 (1983), 647–657.

[DJ06] Donner C., Jensen H. W.: A spectral BSSRDF for shading human skin. In *17th Eurographics Workshop on Rendering* (2006), pp. 409–418.

[dLE07] d'Eon E., Luebke D., Enderton E.: Efficient rendering of human skin. In *18th Eurographics Workshop on Rendering* (June 2007), pp. 147–158.

[DRS07] Dorsey J., Rushmeier H., Sillion F.: *Digital Modeling of Material Appearance*. Morgan Kaufmann, 2007.

[DWd*08] Donner C., Weyrich T., d'Eon E., Ramamoorthi R., Rusinkiewicz S.: A layered, heterogeneous reflectance model for acquiring and rendering human skin. *ACM Transactions on Graphics 27*, 5 (2008), 1–12.

[FBLS05] Fuchs M., Blanz V., Lensch H., Seidel H.: Reflectance from images: a model-based approach for human faces. *IEEE T. Vis. Comput. Gr. 11*, 3 (2005), 296–305.

[Fle00] Flewelling R.: Noninvasive optical monitoring. In *The Biomedical Engineering Handbook*, Bronzino J. D., (Ed.), 2 ed. CRC Press LLC, 2000.

[Fli06] Flindt R.: *Amazing Numbers in Biology*. Springer, 2006.

[Fuc95] Fuchs E.: Keratins and the skin. *Annual Review of Cell and Developmental Biology 11*, 1 (1995), 123–154. PMID: 8689554.

[Ful97] Fulton J.: Utilizing the ultraviolet (uv detect) camera to enhance the appearance of photodamage and other skin conditions. *Dermatol. Surg. 23* (1997), 163–169.

[Gaw02] Gawkrodger D. J.: *Dermatology An Illustrated Colour Text*. Churchill Livingstone, 2002.

[GHP*08] Ghosh A., Hawkins T., Peers P., Frederiksen S., Debevec P.: Practical modeling and acquisition of layered facial reflectance. *ACM Transactions on Graphics 27* (December 2008), 139:1–139:10.

[HASS10] Hansen M., Atkinson G., Smith L., Smith M.: 3D face reconstructions from photometric stero using near infrared and visible light. *Comput. Vis. Image Und. 114* (2010), 942–951.

[Hay05] Laboratory assessment of oxygenation in methemoglobinemia. *Clinical Chemistry 51*, 2 (2005), 434–444.

[HK93] Hanrahan P., Krueger W.: Reflection from layered surfaces due to subsurface scattering. In *Proceedings of the 20th annual conference on Computer graphics and interactive techniques* (August 1993), pp. 165–174.

[HOD*05] Hennessy A., Oh C., Diffey B., Wakamatsu K., Ito S., Rees J.: Eumelanin and pheomelanin concentrations in human epidermis before and after UVB irradiation. *Pigment Cell Research 18* (2005), 220–223.

[INN07] Igarashi T., Nishino K., Nayar S. K.: The appearance of human skin: A survey. *Found. Trends. Comput. Graph. Vis. 3* (January 2007), 1–95.

[Jac96] Jacques S. L.: Origins of tissue optical properties in the UVA, visible, and NIR regions. *OSA TOPS on Adv. in Opt. Imaging and Photon Migration 2* (1996), 364–369.

[Jac01] Jacques S. L.: *Optical absorption of melanin.* Tech. rep., Oregon Medical Laser Center, 2001.

[JAP87] Jacques S. L., Alter C. A., Prahl S. A.: Angular dependence of HeNe laser light scattering by human dermis. *Lasers Life Sci. 1* (1987), 309–333.

[JB03] Jensen H., Buhler J.: Digital face cloning. In *SIGGRAPH Technical Sketches* (2003). 2223b.

[JHM*55a] Jacquez J., Huss J., McKeehan W., Dimitroff J., Kuppenhein H.: Spectral reflectance of human skin in the region 0.7-2.6 μ. *J. Appl. Physiol. 8* (1955), 297–299.

[JHM*55b] Jacquez J., Huss J., McKeehan W., Dimitroff J., Kuppenhein H.: Spectral reflectance of human skin in the region 235-700 mμ. *J. Appl. Physiol. 8* (1955), 212–214.

[JSB*10] Jimenez J., Scully T., Barbosa N., Donner C., Alvarez X., Vieira T., Matts P., Orvalho V., Gutierrez D., Weyrich T.: A practical appearance model for dynamic facial color. *ACM Transactions on Graphics 29* (December 2010), 141:1–141:10.

[JSG09] Jimenez J., Sundstedt V., Gutierrez D.: Screen-space perceptual rendering of human skin. *ACM Transactions on Applied Perception 6*, 4 (2009).

[KB04] Krishnaswamy A., Baranoski G. V. G.: A biophysically-based spectral model of light interaction with human skin. *Computer Graphics Forum 23*, 3 (2004), 331–340.

[KB07] Kimmel B. W., Baranoski G. V. G.: A novel approach for simulating light interaction with particulate materials: application to the modeling of sand spectral properties. *Optics Express 15*, 15 (Jul 2007), 9755–9777.

[KHK*12] Kim M. H., Harvey T. A., Kittle D. S., Rushmeier H., Dorsey J., Prum R., Brady D.: 3D imaging spectroscopy for measuring hyperspectral patterns on solid objects. *ACM Transactions on Graphics 31*, 38 (2012), 38:1–11.

[KR11] Kim M. H., Rushmeier H.: Radiometric characterization of spectral imaging for textual pigment identification. In *12th International Conference on Virtual Reality, Archaeology and Cultural Heritage* (2011), VAST'11, p. 57–64.

[KSZC91] Kollias N., Sayre R. M., Zeise L., Chedekel M. R.: Photoprotection by melanin. *J. Photoch. Photobio. B. 9*, 2 (May 1991), 135–60.

[Lat84] Latimer P.: A wave-optics effect which enhances light absorption by chlorophyll *in vivo*. *Photochemistry and Photobiology 40*, 2 (1984), 193–199.

[LHGC99] Lovell A. T., Hebden J. C., Goldstone J. C., Cope M.: Determination of the transport scattering coefficient of red blood cells. In *Proc. SPIE 3597, Optical Tomography and Spectroscopy of Tissue III* (1999), vol. 3597, pp. 175–182.

[Lis13] Lister T. S.: *Simulating the Color of Port Wine Stain Skin*. PhD thesis, University of Southampton,U.K., February 2013.

[LMRPP75] Lee R., Mathews-Roth M. M., Pathak M. A., Parrish J. A.: The detection of carotenoid pigments in human skin. *J Investig Dermatol 64*, 3 (03 1975), 175–177.

[McC76] McCartney E. J.: *Optics of the atmosphere: Scattering by molecules and particles*. John Wiley & Sons, 1976.

[MK66] Mustakallio K., Korhonen P.: Monochromatic ultraviolet-photography in dermatology. *J. Invest. Dermatol. 47*, 4 (1966), 351–356.

[MTKLL*02] Magnenat-Thalmann N., Kalra P., Luc Leveque J., Bazin R., Batisse D., Querleux B.: A computational skin model: fold and wrinkle formation. *Information Technology in Biomedicine, IEEE Transactions on 6*, 4 (2002), 317–323.

[MTY09] M.F.Yang, Tuchin V., Yaroslavsky A.: Principles of light-skin interactions. In *Light-Based Therapies for Skin of Color* (London, 2009), Baron E., (Ed.), Springer-Verlag, pp. 1–44.

[MWL*99a] Marschner S., Westin S. H., Lafortune E., Torrance K., Greenberg D.: Image-based BRDF measurement including human skin. In *Rendering Techniques'1999* (Granada, June 1999), Lischinski D., Larson G. W., (Eds.), Springer-Verlag, pp. 119–130.

[MWL*99b] Marschner S., Westin S. H., Lafortune E., Torrance K., Greenberg D.: *Reflectance Measurements of Human Skin*. Tech. Rep. PCG-99-2, Program of Computer Graphics, Cornell University, USA, January 1999.

[NL01] Ng C. S.-L., Li L.: A multi-layered reflection model of natural human skin. In *Computer Graphics International 2001* (Washington, DC, USA, 2001), CGI '01, IEEE Computer Society, pp. 249–256.

[NMS10] Nakagawa N., Matsumoto M., Sakai S.: *In vivo* measurement of the water content in the dermis by confocal Raman spectroscopy. *Skin Research and Technology 16*, 2 (2010), 137–141.

[NZS*06] Nielsen K. P., Zhao L., Stamnes J. J., Stamnes K., Moan J.: The importance of the depth distribution of melanin in skin for DNA protection and other photobiological processes. *J. Photoch. Photobio. B. 82*, 3 (2006), 194 – 198.

[OGE73] Olson R. L., Gaylor J., Everett M. A.: Skin color, melanin, and erythema. *Arch. Dermatol. 108*, 4 (1973), 541–544.

[Oud12] Oudhia A.: UV-VIS spectroscopy as a nondestructive and effective characterization tool for II-VI compounds. *Recent Research in Science and Technology 4*, 8 (2012), 109–111.

[OWT*97] Olivarius F. F., Wulf H. C., Therkildsen P., Poulsen T., Crosby J., Norval M.: Urocanic acid isomers: relation to body site, pigmentation, stratum corneum thickness and photosensitivity. *Archives of Dermatological Research 289* (1997), 501–505. 10.1007/s004030050230.

[Pat95] Pathak M.: Functions of melanin and protection by melanin. In *Melanin: Its Role in Human Photoprotection* (Overland Park, Kansas, USA, 1995), L. Zeise M. C., Fitzpatrick T., (Eds.), Valdenmar Publishing Co., pp. 125–134.

[PF97] Pope R. M., Fry E. S.: Absorption spectrum (380–700 nm) of pure water. II. integrating cavity measurements. *Applied Optics 36*, 33 (Nov 1997), 8710–8723.

[Pra99] Prahl S. A.: *Optical absorption of hemoglobin.* Tech. rep., Oregon Medical Laser Center, 1999.

[Pra01] Prahl S. A.: *PhotochemCAD spectra by category.* Tech. rep., Oregon Medical Laser Center, 2001.

[Pra04] Prahl S. A.: *Optical Absorption of Fat.* Tech. rep., Oregon Medical Laser Center, 2004.

[PW74] Palmer K. F., Williams D.: Optical properties of water in the near infrared. *J. Opt. Soc. Am. 64*, 8 (Aug 1974), 1107–1110.

[RBD*04] Randeberg L., Bonesrønning J., Dalaker M., Nelson J., Svaasand L.: Methemoglobin formation during laser induced photothermolysis of vascular skin lesions. *Lasers in Surgery and Medicine 34*, 5 (2004), 414–419.

[RR10] Robertson K., Rees J. L.: Variation in epidermal morphology in human skin at different body sites as measured by reflectance confocal microscopy. *Acta dermatovenereologica 90*, 4 (2010), 368–373.

[San09] Sandidge D.: *Digital Infrared Photography Photo Workshop.* Wiley Publishing, Inc., 2009.

[SANPR72] Siggaard-Andersen O., NÃrgaard-Pedersen B., Rem J.: Hemoglobin pigments. spectrophotometric determination of oxy-, carboxy-, met-, and sulfhemoglobin in capillary blood. *Clinica Chimica Acta 42*, 1 (1972), 85 – 100.

[SCW91] Squier C. A., Cox P., Wertz P. W.: Lipid content and water permeability of skin and oral mucosa. *J Investig Dermatol 96*, 1 (01 1991), 123–126.

[SG81] Sutherland J. C., Griffin K. P.: Absorption spectrum of dna for wavelengths greater than 300 nm. *Radiation Research 86*, 3 (1981), pp. 399–410.

[SGG*09] Stock M., Gerrard M., Gibbons F., Dykstra J., Mahler H., Walsh L., Kulik J.: Sun protection intervention for highway workers: long-term efficacy of uv photography and skin cancer information on men's protective cognitions and behavior. *Ann. Behav. Med. 38* (2009), 225–236.

[SGPF69] Szabo G., Gerald A., Pathak M., Fitzpatrick T. B.: Racial differences in the fate of melanosomes in human epidermis. *Nature 222*, 5198 (06 1969), 1081–1082.

[Shi07] Shimizu H.: *Shimizu's Textbook of Dermatology*. Hokkaido University Press, 2007.

[Sta01] Stam J.: An illumination model for a skin layer bounded by rough surfaces. In *IN PROCEEDINGS OF THE 12TH EUROGRAPHICS WORKSHOP ON RENDERING TECHNIQUES* (2001), Springer-Verlag, pp. 39–52.

[TBS*95] Tearney G. J., Brezinski M. E., Southern J. F., Bouma B. E., Hee M. R., Fujimoto J. G.: Determination of the refractive index of highly scattering human tissue by optical coherence tomography. *Opt. Lett. 20*, 21 (Nov 1995), 2258–2260.

[THW*91] Thody A. J., Higgins E. M., Wakamatsu K., Ito S., Burchill S. A., Marks J. M.: Pheomelanin as well as eumelanin is present in human epidermis. *J Investig Dermatol 97*, 2 (08 1991), 340–344.

[TKK*01] Talreja P., Kasting G., Kleene N., Pickens W., Wang T.-F.: Visualization of the lipid barrier and measurement of lipid pathlength in human stratum corneum. *AAPS PharmSci 3*, 2 (2001), 48–56.

[ToPoIE07] Tuchin V., of Photo-optical Instrumentation Engineers S.: *Tissue optics: light scattering methods and instruments for medical diagnosis*. SPIE PM. SPIE/International Society for Optical Engineering, 2007.

[TOS*03] Tsumura N., Ojima N., Sato K., Shiraishi M., Shimizu H., Nabeshima H., Akazaki S., Hori K., Miyake Y.: Image-based skin color and texture analysis/synthesis by extracting hemoglobin and melanin information in the skin. In *ACM SIGGRAPH 2003 Papers* (New York, NY, USA, 2003), SIGGRAPH '03, ACM, pp. 770–779.

[Var01] Varcoe J. S.: *Clinical Biochemistry: Techniques and Instrumentation : A Practical Course*. World Scientific, 2001.

[VGI94] Vrhel M., Gershon R., Iwan L.: Measurement and analysis of object reflectance spectra. *Color Research and Application 19*, 1 (1994), 4–9.

[VKS*04] Viator J. A., Komadina J., Svaasand L. O., Aguilar G., Choi B., Stuart Nelson J.: A comparative study of photoacoustic and reflectance methods for determination of epidermal melanin content. *Journal of Investigative Dermatology 122*, 6 (06 2004), 1432–1439.

[vVSP*04] van Veen R. L., Sterenborg H., Pifferi A., Torricelli A., Cubeddu R.: Determination of VIS-NIR absorption coefficients of mammalian fat, with time- and spatially resolved diffuse reflectance and transmission spectroscopy. In *Biomedical Topical Meeting* (2004), Optical Society of America, p. SF4.

[WHH88] Williams M. L., Hincenbergs M., Holbrook K. A.: Skin lipid content during early fetal development. *Journal of Investigative Dermatology 91*, 3 (09 1988), 263–268.

[WMP*06] Weyrich T., Matusik W., Pfister H., Bickel B., Donner C., Tu C., McAndless J., Lee J., Ngan A., Jensen H. W., Gross M.: Analysis of human faces using a measurement-based skin reflectance model. In *ACM SIGGRAPH Papers* (New York, USA, 2006), pp. 1013–1024.

[YB06] Yarynovska I. H., Bilyi A.: Absorption spectra of sulfhemoglobin derivatives of human blood. In *Optical Diagnostics and Sensing VI* (2006), Cote G., Priezzhev A., (Eds.), vol. 6094, SPIE, pp. 1–6.

[YBK*12a] Yim D., Baranoski G., Kimmel B., Chen T., Miranda E.: A cell-based light interaction model for human blood. *Comp. Graph. Forum 31*, 2pt4 (May 2012), 845–854.

[YBK*12b] Yim D., Baranoski G., Kimmel B., Chen T., Miranda E.: A cell-based light interaction model for human blood. *Computer Graphics Forum 31*, 2 (2012), 845–854.

[You97] Young A. R.: Chromophores in human skin. *Physics in Medicine and Biology 42*, 5 (1997), 789.

[ZHS04] Zucker S. D., Horn P. S., Sherman K. E.: Serum bilirubin levels in the u.s. population: gender effect and inverse correlation with colorectal cancer. *Hepatology 40*, 4 (Oct 2004), 827–835.